Taylor & Francis
Taylor & Francis Group

Science and Technology of Advanced Materials: Methods

ISSN: (Print) (Online) Journal homepage: www.tandfonline.com/journals/tstm20

Creep data sheet for Nickel-based 19Cr-18Fe-3Mo-5Nb-Ti-Al superalloy

Kota Sawada, Yasushi Taniuchi, Kaoru Sekido, Takehiro Nojima, Tomotaka Hatakeyama & Kazuhiro Kimura

To cite this article: Kota Sawada, Yasushi Taniuchi, Kaoru Sekido, Takehiro Nojima, Tomotaka Hatakeyama & Kazuhiro Kimura (2024) Creep data sheet for Nickel-based 19Cr-18Fe-3Mo-5Nb-Ti-Al superalloy, Science and Technology of Advanced Materials: Methods, 4:1, 2425179, DOI: 10.1080/27660400.2024.2425179

To link to this article: https://doi.org/10.1080/27660400.2024.2425179

Published online: 28 Nov 2024.

SCIENCE AND TECHNOLOGY OF ADVANCED MATERIALS: METHODS
2024, VOL. 4, NO. 1, 2425179
https://doi.org/10.1080/27660400.2024.2425179

Creep data sheet for Nickel-based 19Cr-18Fe-3Mo-5Nb-Ti-Al superalloy

Kota Sawada [a], Yasushi Taniuchi [b], Kaoru Sekido [b], Takehiro Nojima [b], Tomotaka Hatakeyama [a] and Kazuhiro Kimura [a]

[a]Research Center for Structural Materials, National Institute for Materials Science, Tsukuba, Ibaraki, Japan; [b]Research Network and Facility Services Division, National Institute for Materials Science, Tsukuba, Ibaraki, Japan

ABSTRACT

Creep data of Ni-based 19Cr-18Fe-3Mo-5Nb-Ti-Al superalloy (JIS NCF718-B) were obtained at 550°C to 750°C under 100MPa to 1000MPa and analyzed to determine the 100,000 h creep rupture strength. The tensile properties were also evaluated at room temperature to 750°C. Four heats of JIS NCF718-B were used in this study. There was no large difference in the 0.2% proof stress and tensile strength among the heats. A difference in the tensile ductility was observed at 650°C to 750°C among the heats. Heat-to-heat variation of the creep rupture strength was confirmed among the heats and the variation became large in the long term. Regression analysis was conducted for the tensile test data of the four heats. The creep rupture data of all the heats were fitted to the regression equation of logarithmic stress using the time – temperature parameters of Larson – Miller, Orr – Sherby – Dorn, and Manson – Haferd to estimate the 100,000 h creep rupture strength. The Orr – Sherby – Dorn parameter and regression equation of the second degree was suitable for the creep strength evaluation.

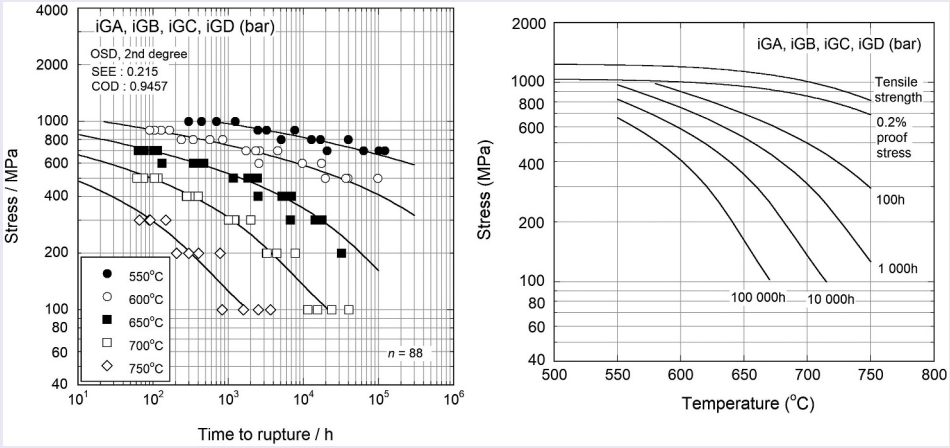

IMPACT STATEMENT

This paper shows long-term creep data and microstructure of creep ruptured specimens for Nickel-based 19Cr-18Fe-3Mo-5Nb-Ti-Al superalloy. The creep rupture data at 550°C to 750°C were expressed by a regression equation using the Orr–Sherby–Dorn parameter.

ARTICLE HISTORY
Received 30 July 2024
Revised 3 October 2024
Accepted 29 October 2024

KEYWORDS
Ni-based superalloy 100 000 h creep rupture strength; heat-to-heat variation

1. Introduction

Ni-based 19Cr-18Fe-3Mo-5Nb-Ti-Al superalloy (JIS NCF718-B) is frequently used for high-temperature components of gas turbines and aircraft engines. The high-temperature strength of the Ni-based superalloy is due to precipitation strengthening facilitated by very fine γ”-Ni_3Nb and γ’-Ni_3(Al, Ti) particles. Because the γ” phase is metastable, it changes to a stable δ phase (Ni_3Nb) during long-term aging. The shape of the δ phase is needlelike. Allowable stress based on the tensile and creep properties is normally needed to design high-temperature components. Especially in the case of very high temperatures, the creep property dominates the allowable stress. The long-term creep rupture strength should be evaluated to determine the allowable stress, for which the criterion is normally the 100,000 h creep rupture strength [1,2]. In many cases, the 100,000 h creep rupture strength is extrapolated from the short-term creep rupture data. On the other hand, in some cases, the extrapolation is not successful since premature creep

CONTACT Kota Sawada SAWADA.Kota@nims.go.jp Research Center for Structural Materials, National Institute for Materials Science, 1-2-1 Sengen, Tsukuba, Ibaraki, Japan

fracture occurs. Therefore, the creep rupture strength should be evaluated based on long-term creep data, considering the trend of the creep rupture data. The National Institute for Materials Science recently obtained long-term creep rupture data for Ni-based 19Cr-18Fe-3Mo-5Nb-Ti-Al superalloy (JIS NCF718-B) for the NIMS Creep Data Sheet Project.

In the present study, we evaluated the tensile and creep properties and estimated the 100,000 h creep rupture strength of Ni-based 19Cr-18Fe-3Mo-5Nb-Ti-Al superalloy (JIS NCF718-B).

2. Experimental procedures

2.1. Material

The material examined was Ni-based 19Cr-18Fe-3Mo-5Nb-Ti-Al superalloy (NCF718-B; JIS G 4901–1999 [3]). Details such as the type of melting, product form, processing, and thermal history are listed in Table 1. Four commercial heats, iGA, iGB, iGC and iGD, were sampled from several companies for tensile and creep testing. In the NIMS Creep Data Sheet Project, several commercial heats are normally selected because the users of the material need to know the heat-to-heat variation of the creep strength to design components. Table 2 shows the chemical compositions of the four heats. All the compositions were within the range of specifications of JIS G 4901–1999 [3].

2.2. Tensile and creep testing

Tensile testing was conducted at temperatures ranging from 24°C to 750°C in accordance with JIS G 0567 [4]. The engineering (nominal) strain rate of the specimens was controlled to 5×10^{-5} s^{-1} up to about 1.0% proof stress and 1.25×10^{-3} s^{-1} beyond that.

Table 1. Details of 19Cr-18Fe-3Mo-5Nb-Ti-Al superalloy bars[1].

NIMS reference code	Type of melting[2)]	Size of ingot (kg)	Deoxidation process[3)]	Product form	Dimensions [4)] (mm)	Processing and thermal history[5)]	Austenite grain size number[6)]	Rockwell harndess (HRC)
iGA	VIM VAR	2000	VOD	Bar	25D 1000 L	Forged 970°C/2 h WQ test specimen only 960°C/ 50 min Ar 720°C/8 h 625°C/9.5 h Ar → AC	4.6	42
iGB		2950			50D	Hot rolling 982°C/12.3 min WQ test specimen only 960°C/50 min Ar 720°C/ 8h625°C/9.5 h Ar → AC	8.6	45
iGC	CE ESR	2000			25D 2000 L	Hot rolling 980°C/1 h OQ test specimen only 720°C/8 h 620°C/8.2 h N_2	8.4	46
iGD		1000	VOD RSM		22D	Forged 960°C/1 h ACtest specimen only 720°C/8 h 620°C/8 h Ar	8.2	45

[1)]The bars were sampled in 2000, 2001 and 2002. The details other than grain size number and hardness were reported by the steel manufacturer.
[2)]VIM : vacuum induction melting furnace, VAR : vacuum arc remelting furnace, ESR : electroslag remelting furnace.
[3)]VOD : vacuum oxygen decarburization and deoxidation, RSM : refining slag mixing.
[4)]D : diameter, L : length.
[5)]WQ : water quenching, Ar : argon cooling, FC : furnace cooling, AC : air cooling, OQ : oil quenching, N2 : nitrogen cooling.
[6)]JIS G 0551–2020, 'Steel-Micrographic determination of the apparent grain size'

Table 2. Chemical composition (product analysis) of Nickel based 19Cr-18Fe-3Mo-5Nb-Ti-Al superalloy bars.

	Chemical composition (mass percent) [1)]										
NIMS reference code	C	Si	Mn	P	S	Ni	Cr	Mo	Cu	Ti	Al
JIS[2)]	≤0.08	≤0.35	≤0.35	≤0.015	≤0.015	50.00-55.00	17.00-21.00	2.80-3.30	≤0.30	0.65-1.15	0.20-0.80
ASME code [3)]	≤0.08	≤0.35	≤0.35	≤0.015	≤0.015	50.0-55.0	17.0-21.0	2.80-3.30	≤0.30	0.65-1.15	0.20-0.80
iGA	0.045	0.077	0.056	0.002	0.001	53.5	17.6	3.11	0.005	0.97	0.58
iGB	0.034	0.096	0.068	0.010	<0.001	52.9	17.4	3.0	0.038	0.95	0.51
iGC	0.029	0.079	0.032	0.001	<0.001	52.3	18.0	3.00	0.006	0.94	0.55
iGD	0.039	0.18	0.09	0.004	0.001	52.7	19.08	3.00	0.01	0.88	0.53

NIMS reference code	B	Nb+Ta	Fe
JIS[2)]	≤0.006	4.75-5.50	bal.
ASME code [3)]	≤0.006	4.75-5.50	bal.
iGA	0.0025	5.00	bal.
iGB	0.0024	5.32	bal.
iGC	0.0035	5.15	bal.
iGD	0.0034	5.07	bal.

[1)]The chemical composition given above was reported by NIMS except for the elements of the heat iGD, which was reported by the steel manufacturer.
[2)]JIS G 4901–1999, 'Corrosion-resisting and heat-resisting superalloy bars'
[3)]ASME SB-637, 2023. SPECIFICATION FOR PRECIPITATION-HARDENING AND COLD WORKED NICKEL ALLOY BARS, FORGINGS, AND FORGING STOCK FOR MODERATE OR HIGH-TEMPERATURE SERVICE.

Creep testing at 550°C to 750°C was performed in accordance with JIS Z 2271 [5]. Creep strain – time data were obtained using five hundred single-type creep testing machines developed by NIMS. Solid cylindrical specimens with gauge mark projections were used as shown in our previous study [6]. Specimens with a gauge diameter of 6 mm and 10 mm were used depending on the testing temperature as shown in Figure 1. The number of specimens for creep test was 22 for each heat.

2.3. Temperature measurement and control

The degree of temperature used in the tensile and creep testing was based upon the International Temperature Scale of 1990 [7]. The temperature was maintained to within ± 3°C for temperatures equal to or higher than 100°C but equal to or lower than 750°C.

2.4. Microstructure observation

For observation by optical microscope, the creep-ruptured specimens were cut longitudinally parallel to the stress direction using a water-cooled fine cutter, then embedded in hard resin, and then polished with emery paper and buffing cloths with paste. The samples were etched with 1 g $CuCl_2$, 20 ml HCl, and 30–50 ml C_2H_5OH. The etching temperature was changed depending on the creep test conditions. For observation by scanning electron microscope, the samples were polished with emery paper and buffing cloths with paste containing diamond particles, and chemically-mechanically polished with colloidal silica.

3. Analysis methods

3.1. Tensile data

Regression analysis of the tensile data was conducted using the following equation:

$$log\left(S_y \text{ or } S_T\right) = a_0 + a_1 T + a_2 T^2 + \ldots + a_k T^k \quad (1)$$

where S_y = 0.2% proof stress (MPa),
S_T = tensile strength (MPa),
T = temperature (°C),
$a_0, a_1, a_2, \ldots, a_k$ = regression coefficients estimated by the least squares method, and
k = degree of regression equation.

3.2. Creep rupture data

Regression analysis of the creep rupture data was performed using a regression equation of logarithmic stress with the time – temperature parameters (P) of Larson – Miller (LM) [8], Orr – Sherby – Dorn (OSD) [9], and Manson – Haferd (MH) [10] as follows:

$$\text{LM } P = (T + 273.15)(C + logt_R) \quad (2)$$

$$\text{OSD } P = log\ t_R - Q/[2.3R(T + 273.15)] \quad (3)$$

$$\text{MH } P = (log\ t_R - log\ t_a)/(T + 273.15 - T_a) \quad (4)$$

where t_R = time to rupture (h),

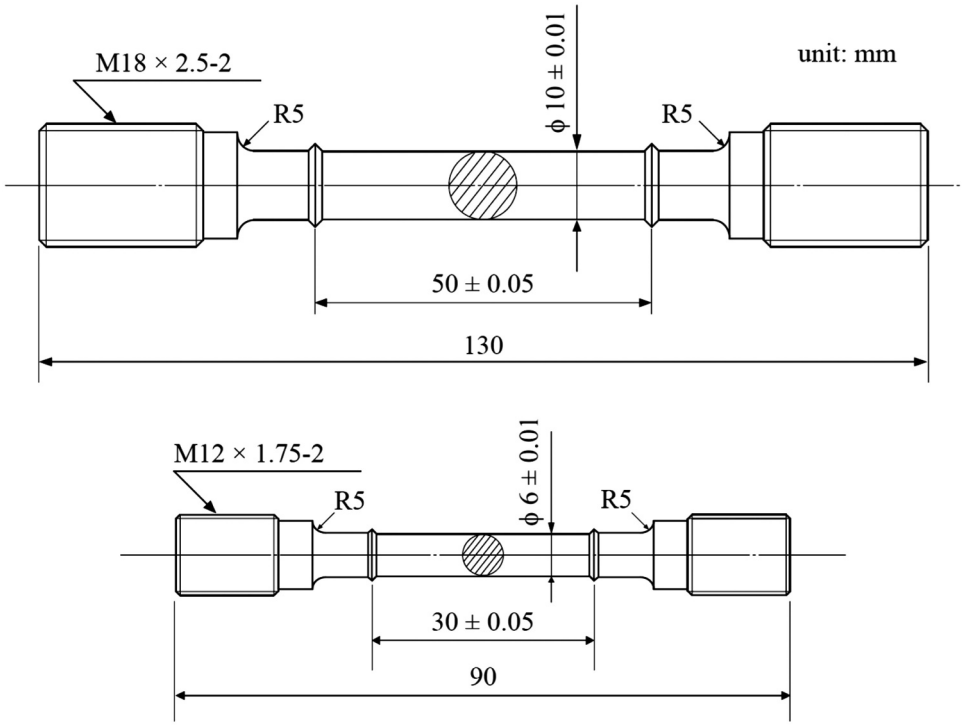

Figure 1. Specimens for tensile and creep tests.

T = temperature (°C),
C, Q, t_a, and T_a = optimized constants, and
R = gas constant.

There are also many time-temperature-parameters except for the parameters mentioned above [11]. The master creep rupture curve equations for the fit were of the following form:

$$P = b_0 + b_1 log\ \ S + b_2(log\ S)^2 + \ \ldots\ + b_k(logS)^k \tag{5}$$

$$P = b + b_0 S + b_1 log\ S + b_2(log\ S)^2 + \ \ldots\ + b_k(logS)^k \tag{6}$$

where S = stress (MPa),
b, b_0, b_1, b_2, b_3, ... , b_k = regression coefficients estimated by the least squares method, and k = degree of regression equation.

4. Experimental results

4.1. Initial microstructure and tensile properties

Optical micrographs of the as-received samples are shown in Figure 2. The grain size of the iGA heat is apparently larger than that of the other heats. Layered contrasts are observed along the longitudinal direction of the bar in all heats. For the iGD heat, the layered contrasts may have originated from the mixed grain structure. The dark and light contrasts correspond to the fine and coarse grain areas, respectively. The layered contrast is relatively strong in the iGD heat compared to the other heats. In some cases, solidifying segregation cannot be completely eliminated during the manufacturing process. The remaining segregation along the longitudinal direction of the bar can be one of the reasons for the formation of a layered structure [12].

The tensile properties of the four heats are shown in Figure 3. The tensile strength and 0.2% proof stress gradually decreased with an increase in the test temperature for the four heats. There was no large difference in the tensile strength and 0.2% proof stress among the heats. On the other hand, the temperature dependence of the tensile ductility was not observed up to 600°C for the four heats. However, the heat-to-heat variation in the tensile ductility became large at 650°C to 750°C. The ductility of the iGB heat was

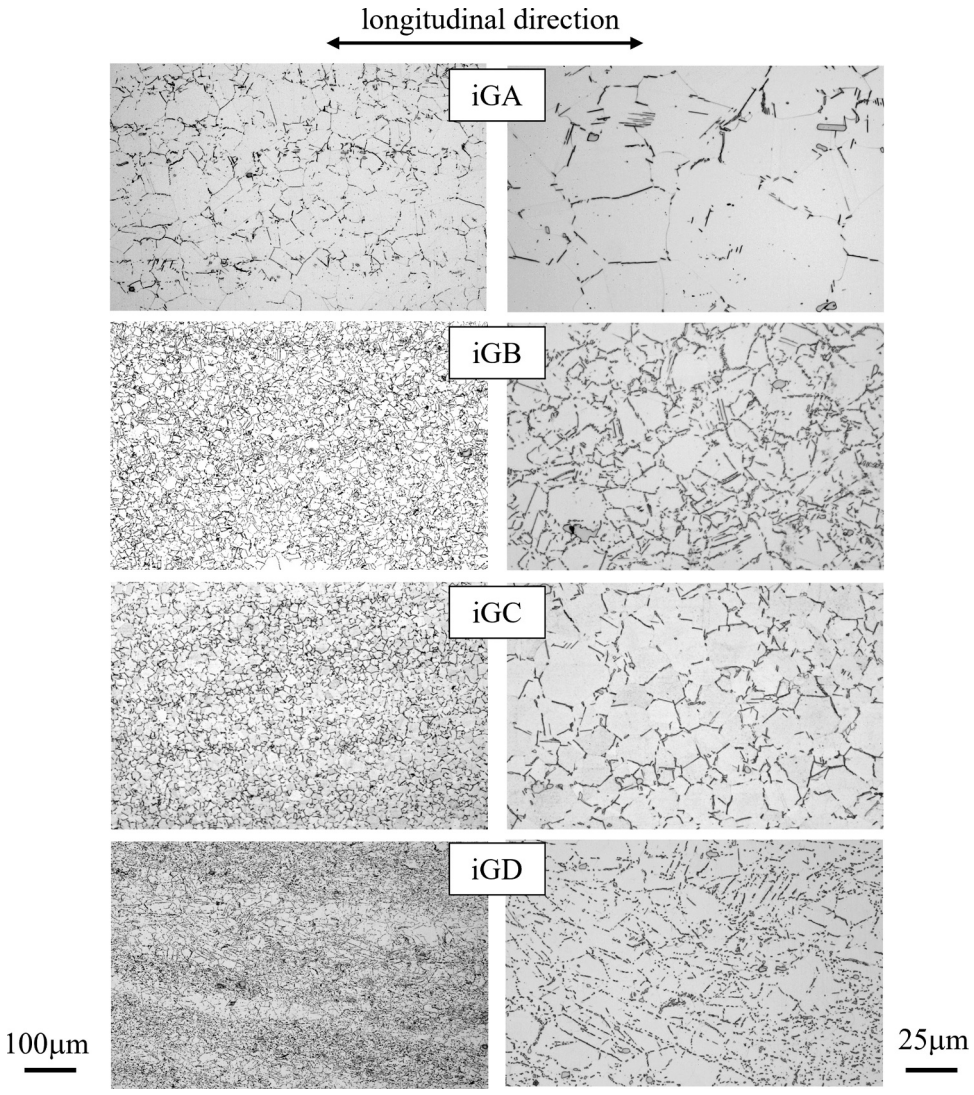

Figure 2. Optical micrographs of as-received nickel based 19Cr-18Fe-3Mo 5Nb-Ti_A1 superalloy bars.

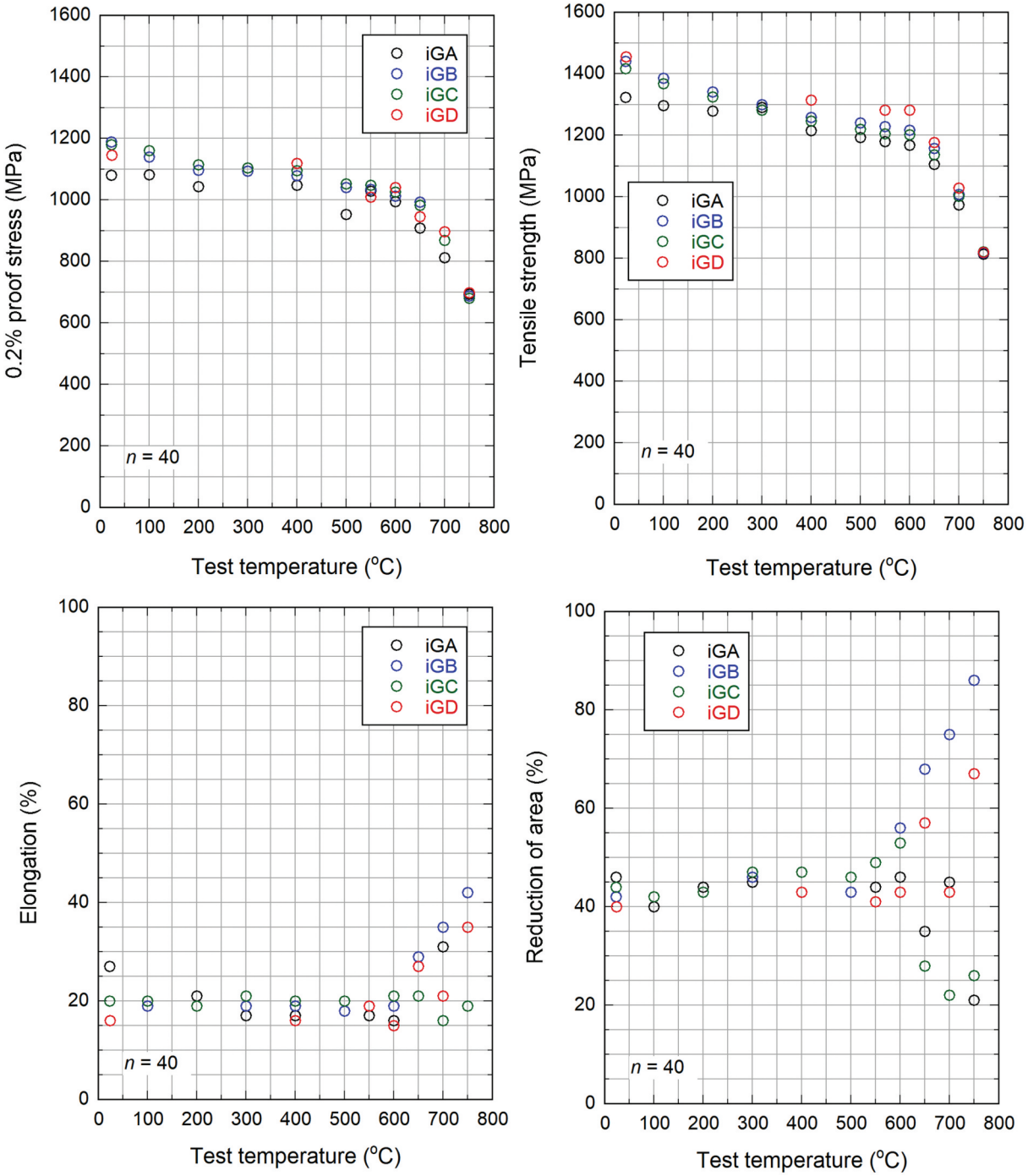

Figure 3. Tensile properties at various temperatures (a) 0.2% proof stress, (b) tensile strength, (c)elongation, (d) reduction of area.

larger than that of the other heats at these temperatures. The grain size number was relatively large in the iGB heat compared to the other heats, as shown in Table 1. This may be one of the reasons for the high ductility at 650°C to 750°C. Grain boundary sliding can easily occur when gain size is fine, which contributes to the high ductility. The difference of grain size can not explain the low elongation of iGC at 700°C and 750°C because the grain size of iGC is almost the same as that of iGD. The γ" phase can precipitate 700°C and 750°C during tensile testing. There is possibility that kinetics of γ" phase formation can depend on heats. The heat-to-heat variations of reduction of area at 700°C and 750°C may be attributed to the difference of kinetics of γ" phase. The detail will be investigated in future work.

4.2. Creep properties

Figure 4 demonstrates the stress versus the time to rupture curve at 550°C to 750°C. The heat-to-heat variation in the creep strength was clearly confirmed at each temperature. The creep strength of the iGD heat was lower than that of the other heats at all testing temperatures. At 700°C and 750°C, the creep strength of the iGA heat was apparently higher than that of the

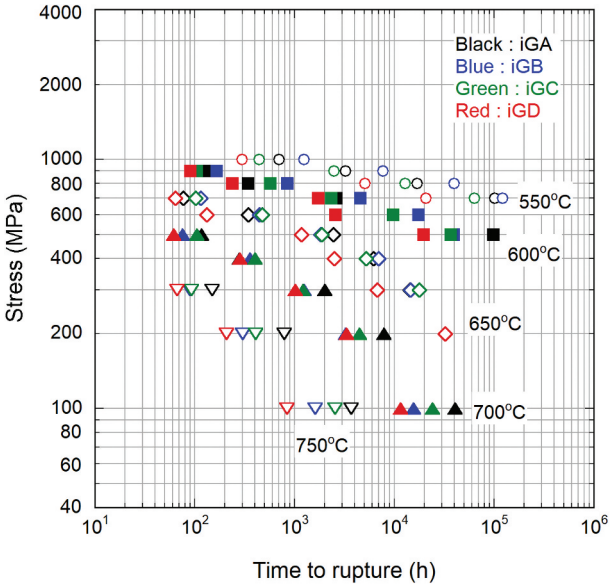

Figure 4. Creep rupture strength of all heats.

other heats. The grain size number of iGA was much lower than that of the other heats, as shown in Table 1. It was reported that the creep strength can be high when the grain size is large corresponding to a low grain size number [13,14]. Therefore, the high creep strength of iGA can be attributed to the low grain size number. The difference in the creep strength among the heats became large in the long term, indicating that the microstructural change during creep exposure differed among the heats. The results of microstructure observation are discussed later. Elongation and reduction of the area for creep-ruptured specimens are shown in Figures 5 and 6, respectively. Basically, the elongation and reduction of area became larger at higher testing temperatures for all the heats. There was heat-to-heat variation in the creep rupture ductility at all testing temperatures. However, the tendency of a change in the creep ductility was not confirmed at 550°C to 650°C. On the other hand, at 700°C and

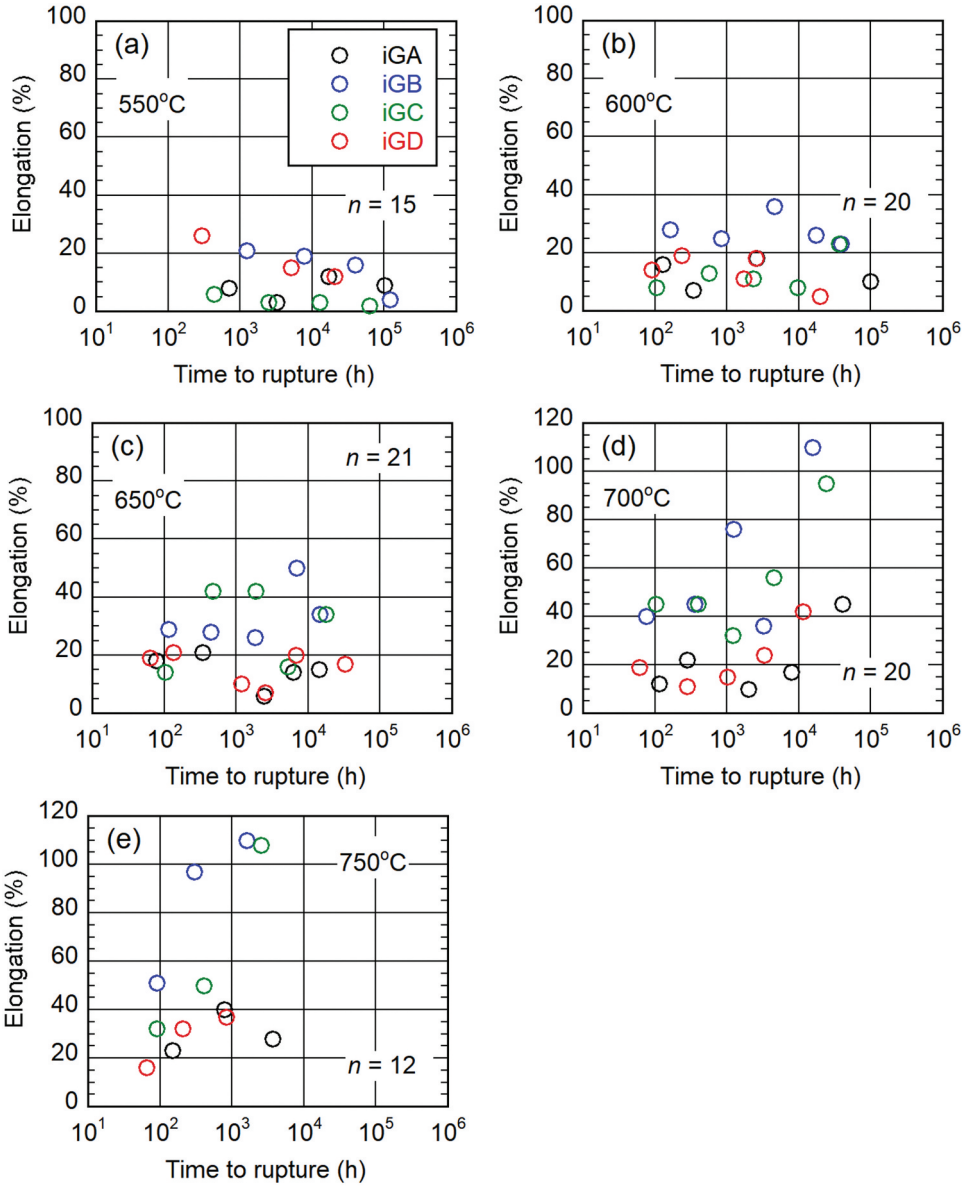

Figure 5. Elongation of creep ruptured samples. (a) 550°C, (b) 600°C, (c) 650°C, (d) 700°C, (e) 750°C.

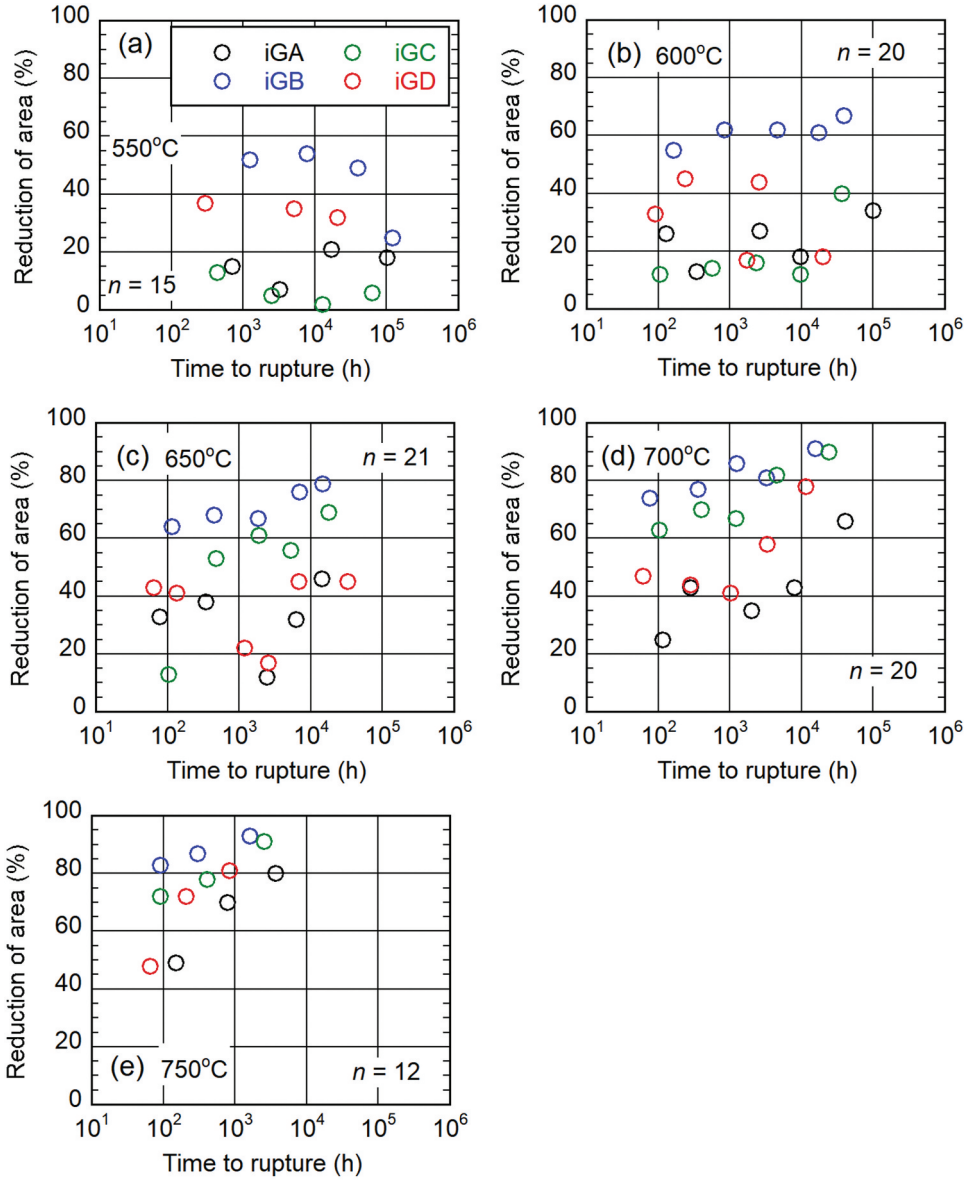

Figure 6. Reduction of area of creep ruptured samples. (a) 550°C, (b) 600°C, (c) 650°C, (d) 700°C, (e) 750°C.

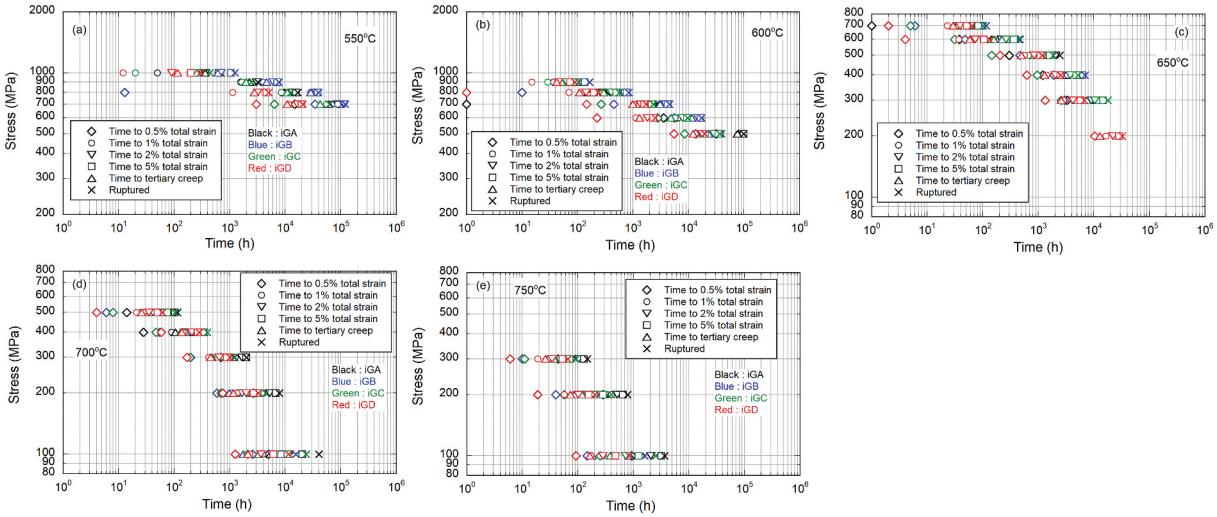

Figure 7. Time to reach specified total strain, time to tertiary creep and time to rupture. (a) 550°C,(b) 600°C, (c) 650°C, (d) 700°C, (e) 750°C.

750°C, the creep ductility of iGA was lower than that of the other heats. This could be due to the low grain size number of iGA, as shown in Table 1. Figure 7 shows the time to reach the specified total strain and

the time to the initiation of tertiary creep. The data were obtained from creep curves under all testing conditions. The time to the initiation of tertiary creep means the time to the 0.2% offset strain of the tertiary creep. The stress dependence of the minimum creep rate is shown in Figure 8. The stress dependence decreased with an increase in the testing temperature. Normally, the stress dependence can be large when the precipitation strengthening contributes to the creep strength. Therefore, the decrease in stress dependence shown in Figure 8 indicates a decrease in the precipitation strengthening at higher temperatures. At 700°C and 750°C, the minimum creep rate of iGA was apparently lower than that of the other heats at the same stress level. The low grain size number of iGA is one of the reasons for the low minimum creep rate. The Monkman – Grant relationship [15] and the regression coefficient of the linear relationship are shown in Figure 9 and Table 3, respectively.

4.3. Microstructure of creep-ruptured samples

Figure 10 shows optical micrographs of the gauge portion of creep-ruptured samples. The specimen with the longest time to rupture in this study was selected for microstructural observation at each temperature. The grain boundaries were relatively clear for iGA, iGB, and iGC compared to iGD. In iGD, the grain boundary was difficult to see due to the formation of many precipitates, as mentioned later. Enlarged optical micrographs of the gauge portion of creep-ruptured samples are shown in Figure 11. At 550°C, needlelike precipitates were observed at the grain boundaries in iGA, iGB, and iGC. The needlelike precipitates had also formed in the grain interior at 600°C to 750°C for iGA, iGB, and iGC. The alloys studied were heat treated for about 1 h at 960–982°C, as shown in Table 1. According to the TTP diagram [16] of NCF718, the δ phase can form at the grain boundaries after 1 h at 960–982°C. Therefore, many of the needlelike precipitates at the grain boundaries may

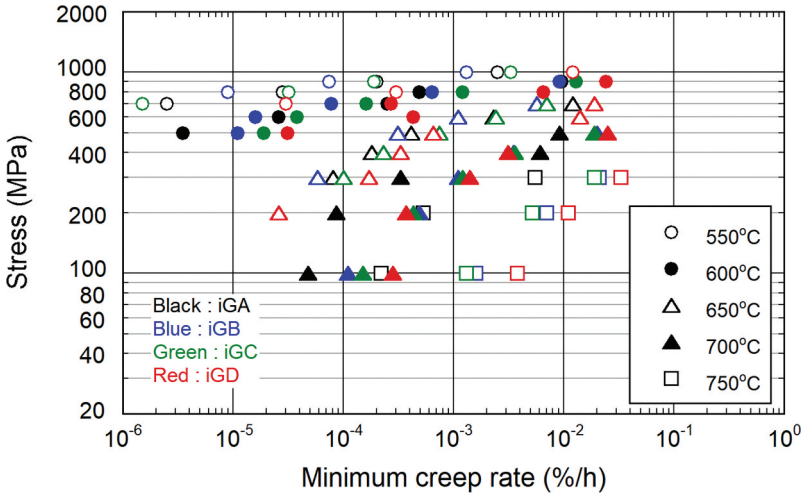

Figure 8. Stress versus minimum creep rate for all heats.

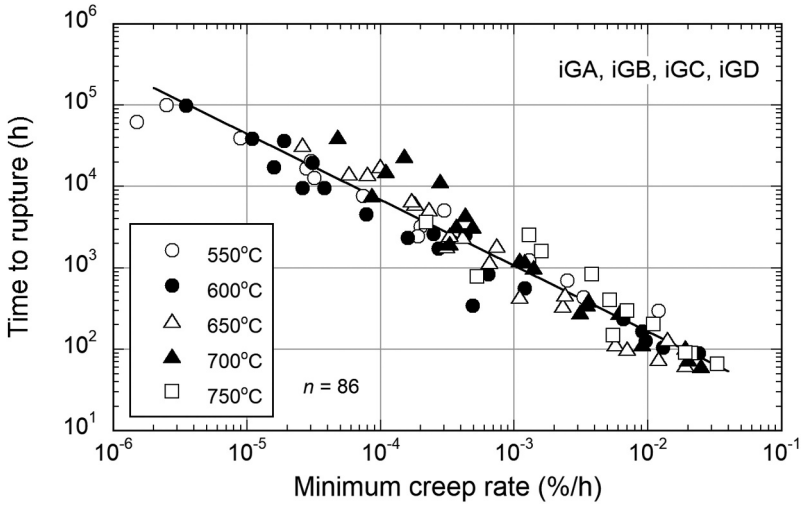

Figure 9. Monkman-Grant relations for all heats.

Table 3. Regression coefficient of the linear relationship between time to rupture and minimum creep rate for Nickel based 19Cr-18Fe-3Mo-5Nb-Ti-Al superalloys.

	log $t_R = A + B$log(minimum creep rate)				
NIMS reference code	n*1	A	B	SEE*2	COD*3
iGA, iGB, iGC, iGD	86	5.970116×10^{-1}	-8.103161×10^{-1}	0.243	0.9259

*1 n : number of data points.
*2 SEE : standard error of estimate.
*3 COD : coefficient of determination.
Minimum creep rate : %/h.
t_R : time to rupture (h).

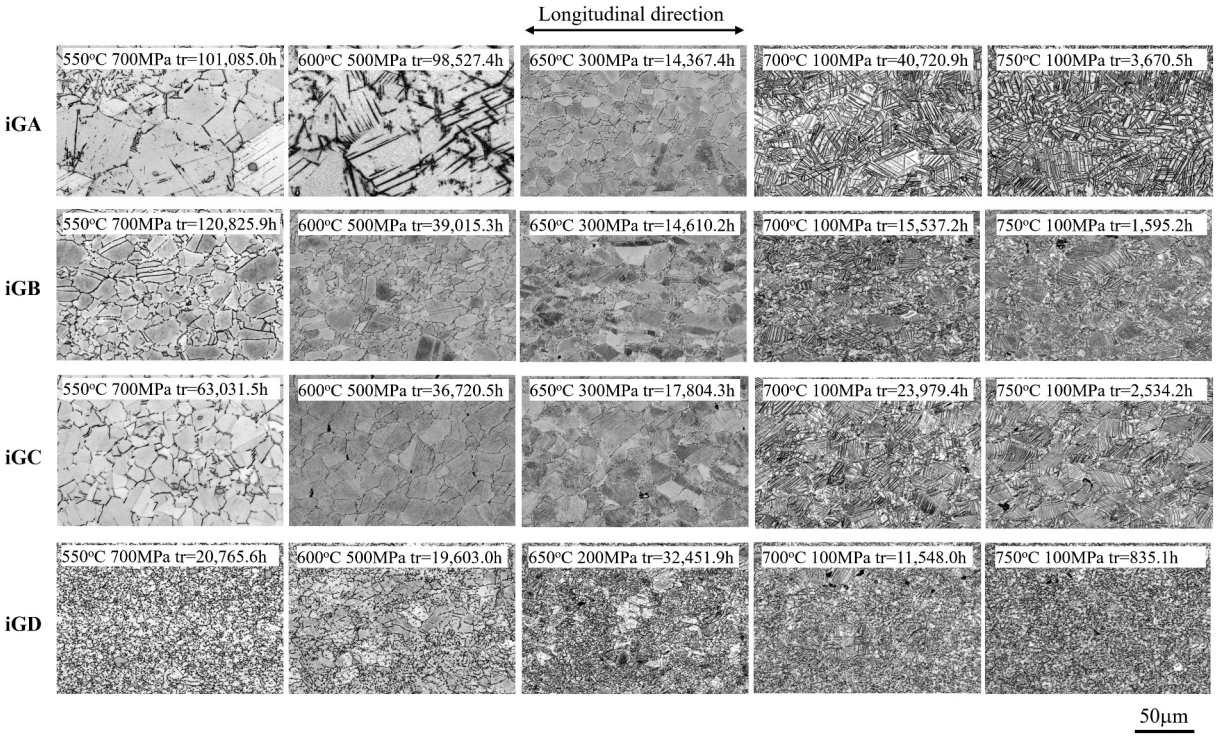

Figure 10. Optical micrographs of gauge portion of creep ruptured samples.

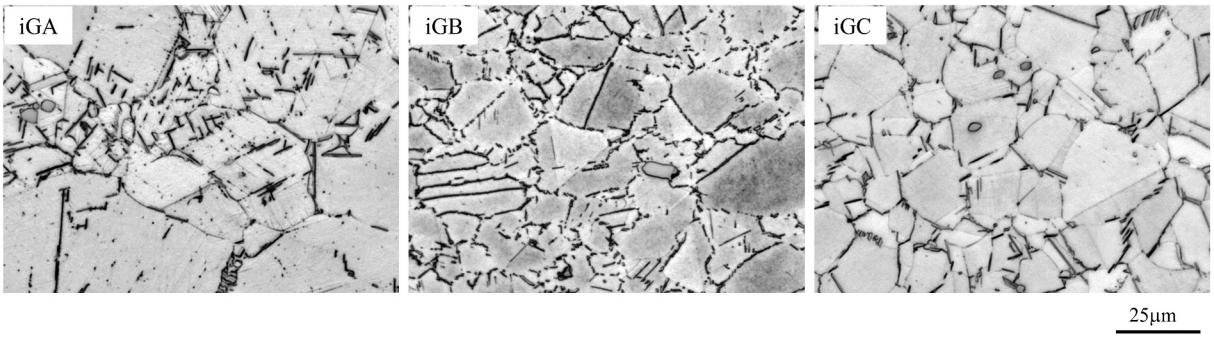

Figure 11. Optical micrographs of gauge portion of creep ruptured samples. iGA : 550°C 700MPa tr = 101,085h. iGB : 550°C 700MPa tr = 120,825.9h. iGC : 550°C 700MPa tr = 63,031.5h.

be the δ phase that formed during the heat treatment. The needlelike precipitates in the grain interior at 700°C and 750°C may also be the δ phase, which can precipitate during aging after 3000 h and 10,000 h at 700°C and 750°C, respectively [16]. SEM micrographs of creep-ruptured samples are shown in Figure 12. In iGD, relatively short needlelike precipitates were observed at the grain boundaries and grain interior although long needlelike precipitates were formed in the other heats. The creep strength of iGD was smaller than that of the other heats, as shown in Figure 4. The difference in the length of the needlelike precipitates may have caused the difference in the creep strength. At 700°C and 750°C, fine grains were observed around the grain boundaries compared to that at lower temperatures. This may indicate that dynamic recrystallization occurred at 700°C and 750°C after long-

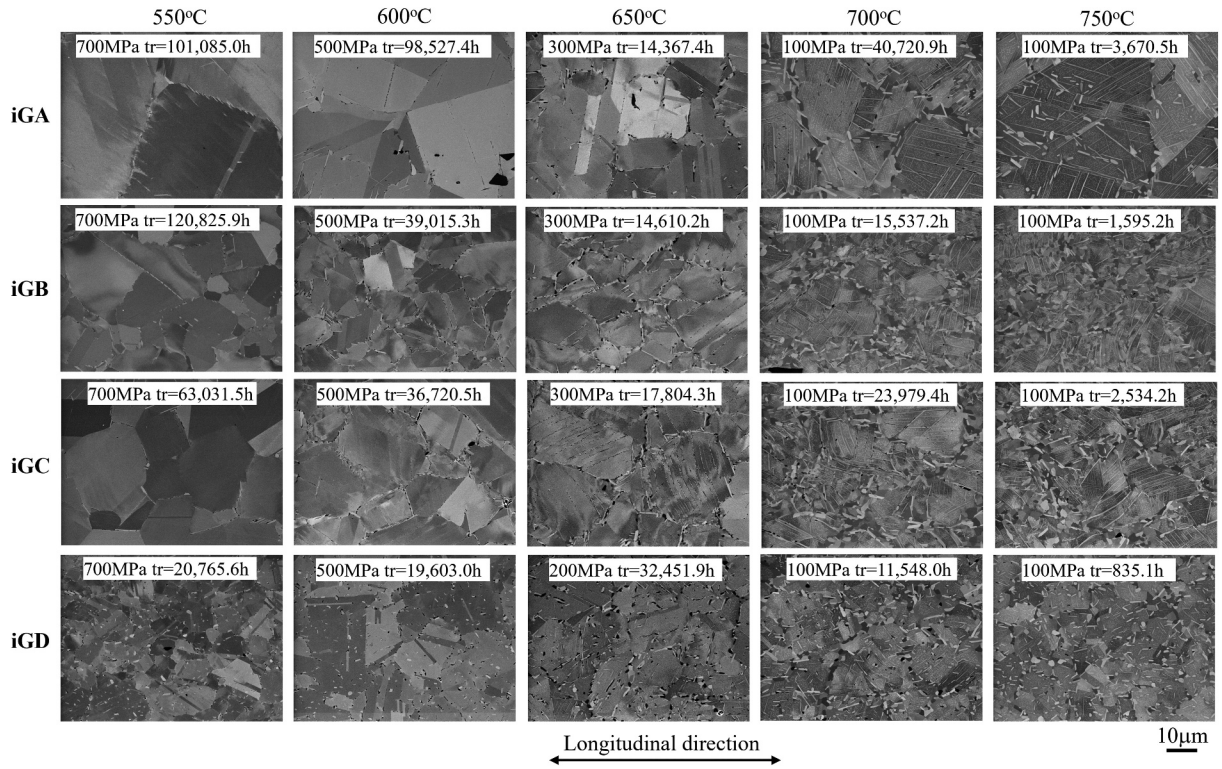

Figure 12. SEM microstructure of guage portion of creep ruptured samples.

term creep. The creep strength degradation in the long term at 700°C and 750°C shown in Figure 4 is attributed to the dynamic recrystallization because the recrystallization can eliminate dislocations and make softening zone. Figure 13 shows a high magnification image of the gauge portion of a creep-ruptured sample at 750°C. Arrows show the γ" or γ' phases. These phases were observed in all heats. It was easy to see the γ" or γ' phases in the grain interior due to their coarseness after long-term creep.

5. Analysis of experimental data

5.1. Analysis of short-term tensile data

Figure 14 shows the results of the regression analysis of the tensile properties. The third, fourth, and fifth degree of the regression Equation (1) were used in an attempt to express the trend of the 0.2% proof stress and tensile strength. The fitting curve using the third degree decreased with an increase in the temperature

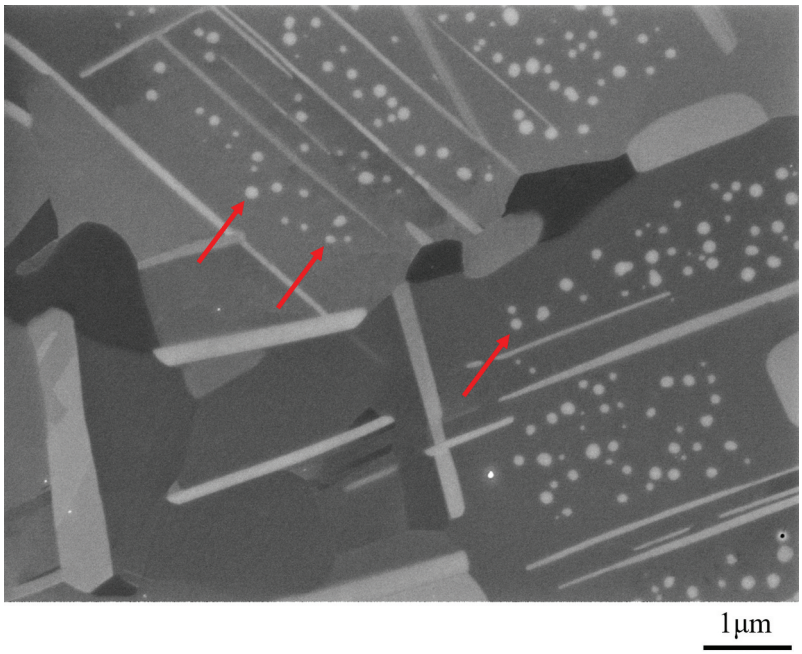

Figure 13. SEM microstructure of guage portion of creep ruptured sample for iGA. 750°C, 100MPa, tr= 3670.5h Arrows indicate γ" or γ' phases.

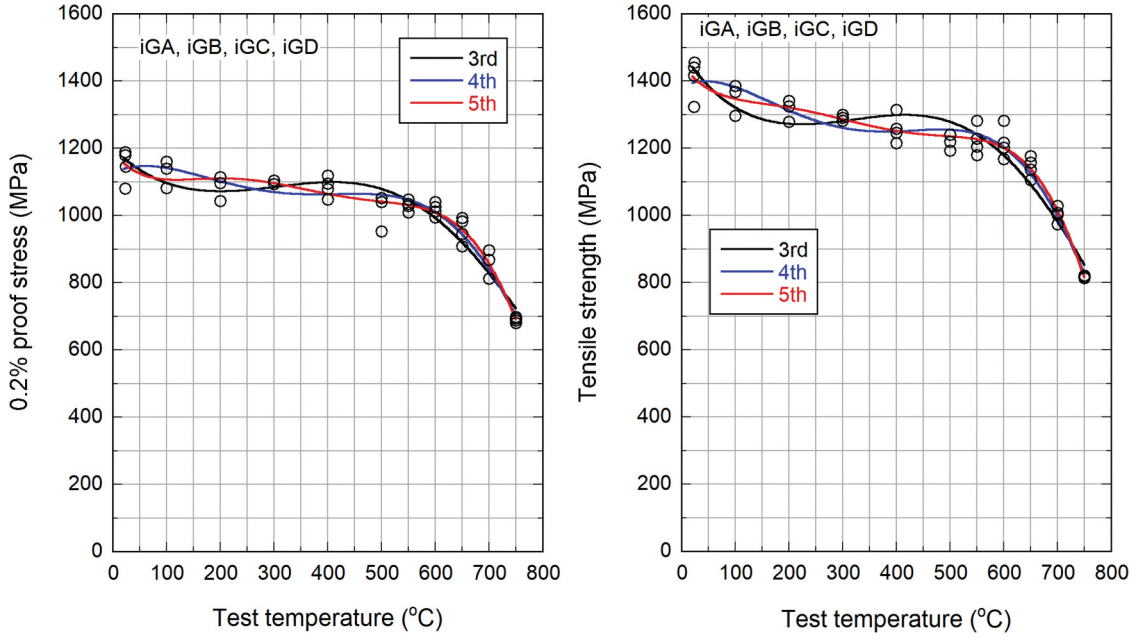

Figure 14. Result of regression analysis of third, fourth and fifth degree for 0.2% proof stress and tensile strength.

Table 4. Summary of polynomial regression for short term tensile properties of Nickel based 19Cr-18Fe-3Mo-5Nb-Ti-Al superalloys.

$\log(S_y \text{ or } S_T) = a_0 + a_1T + a_2T^2 + a_3T^3 + a_4T^4 + a_5T^5$

NIMS reference code	Dependent variable	a_0	a_1	a_2	a_3
iGA, iGB, iGC, iGD	log S_y*3	3.07667	-7.86010×10^{-4}	6.72955×10^{-6}	-2.50699×10^{-8}
	log S_T*4	3.16149	-6.44974×10^{-4}	4.79311×10^{-6}	-1.84887×10^{-8}
	a_4	a_5	SEE*1	COD*2	
	4.05367×10^{-11}	-2.39468×10^{-14}	0.015	0.9782	
	3.18074×10^{-11}	-1.99194×10^{-14}	0.012	0.9853	

*1 SEE : standard error of estimate.
*2 COD : coefficient of determination.
*3 S_y : 0.2% proof stress (MPa).
*4 S_T : tensile strength (MPa).

up to 200°C and increased again at temperatures higher than 200°C. However, the experimental plots showed that the 0.2% proof stress and tensile strength decreased with an increase in the test temperature. Therefore, the fitting curve using the third degree is not suitable for both the 0.2% proof stress and tensile strength. The fitting curve using the fourth degree overestimated the experimental data at room temperature to 200°C. Consequently, the fitting curve using the fifth degree was selected for both the 0.2% proof stress and tensile strength. The value of the regression coefficient is shown in Table 4.

5.2. Analysis of creep rupture data

In this section, the parameters of Larson – Miller (LM) [8], Orr – Sherby – Dorn (OSD) [9], and Manson – Haferd (MH) [10] were used for the analysis of creep rupture data. We selected most useful parameter from three parameters mentioned above. Other parameters [11] were not tried in this study.

The creep rupture data for the four heats were analyzed by Eqs. (2) to (6). Figure 15 shows the results of the regression analysis using the LM parameter and Eq. (5). The fitting curves using the regression equations of the second, fourth and fifth degrees could not express the experimental data at 700°C and 750°C in the long term. It seems that the fitting curve using the third degree can express the experimental data at 700°C and 750°C. In this case, the third degree was relatively accurate although the fitting curve was an S-shape and did not agree with the tendency of the experimental data. The fitting curves using the LM parameter and Eq. (6) are shown in Figure 16. The fitting curves were not suitable when the degree was fourth and fifth for the regression analysis. The fitting curves using the second and third degrees seemed to express the experimental data. The second degree was suitable in this case because of the simplicity of the equation. Figure 17 demonstrates the results of the regression analysis using the OSD parameter and Eq. (5). The fitting curves using the second, fourth, and fifth degrees could not express the experimental data in the long

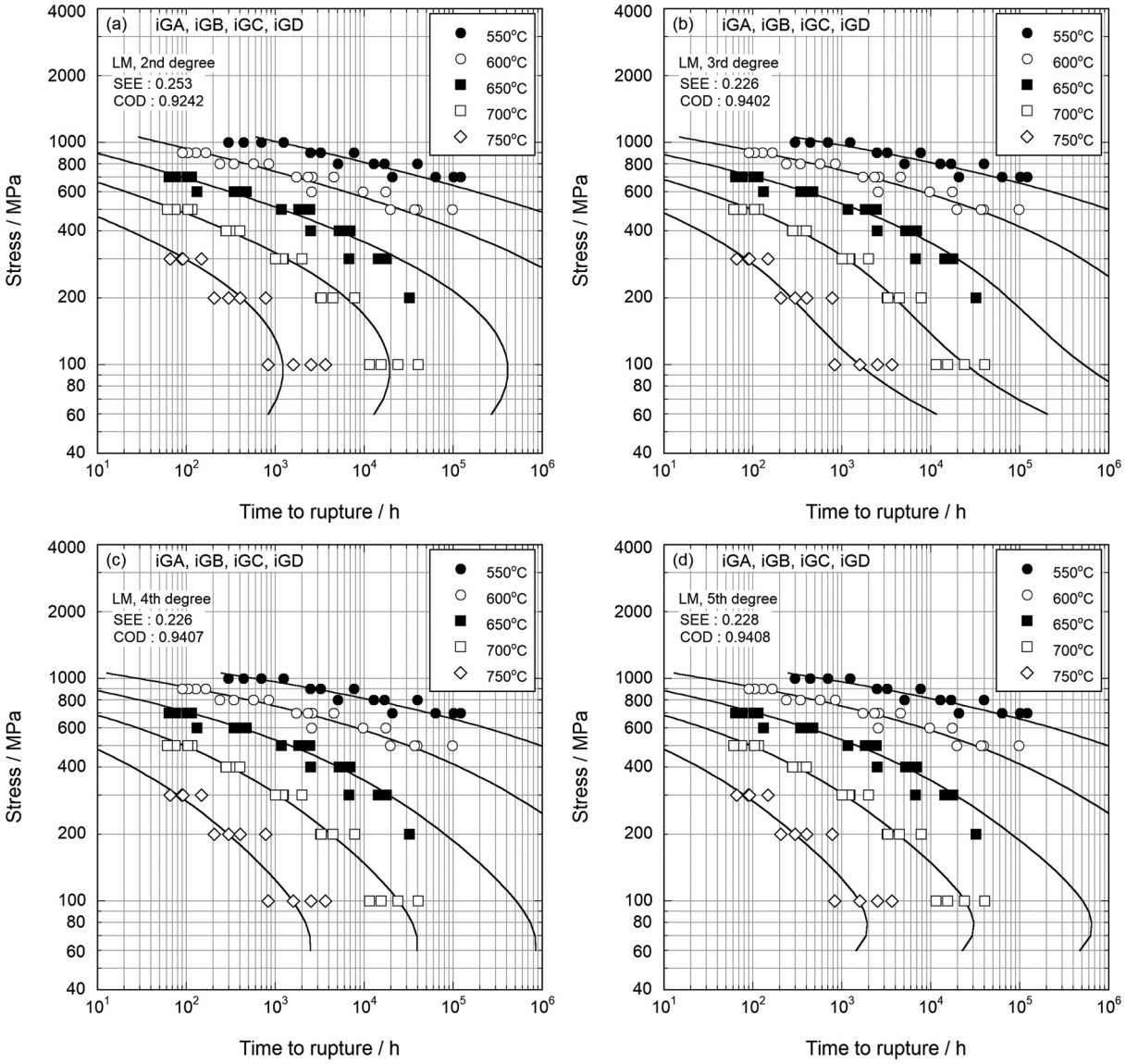

Figure 15. Result of regression analysis by LM parameter and equation (5). (a) 2nd degree, (b) 3rd degree, (c) 4th degree, (d) 5th degree. SEE: standard error of estimate, COD: coefficient of determination.

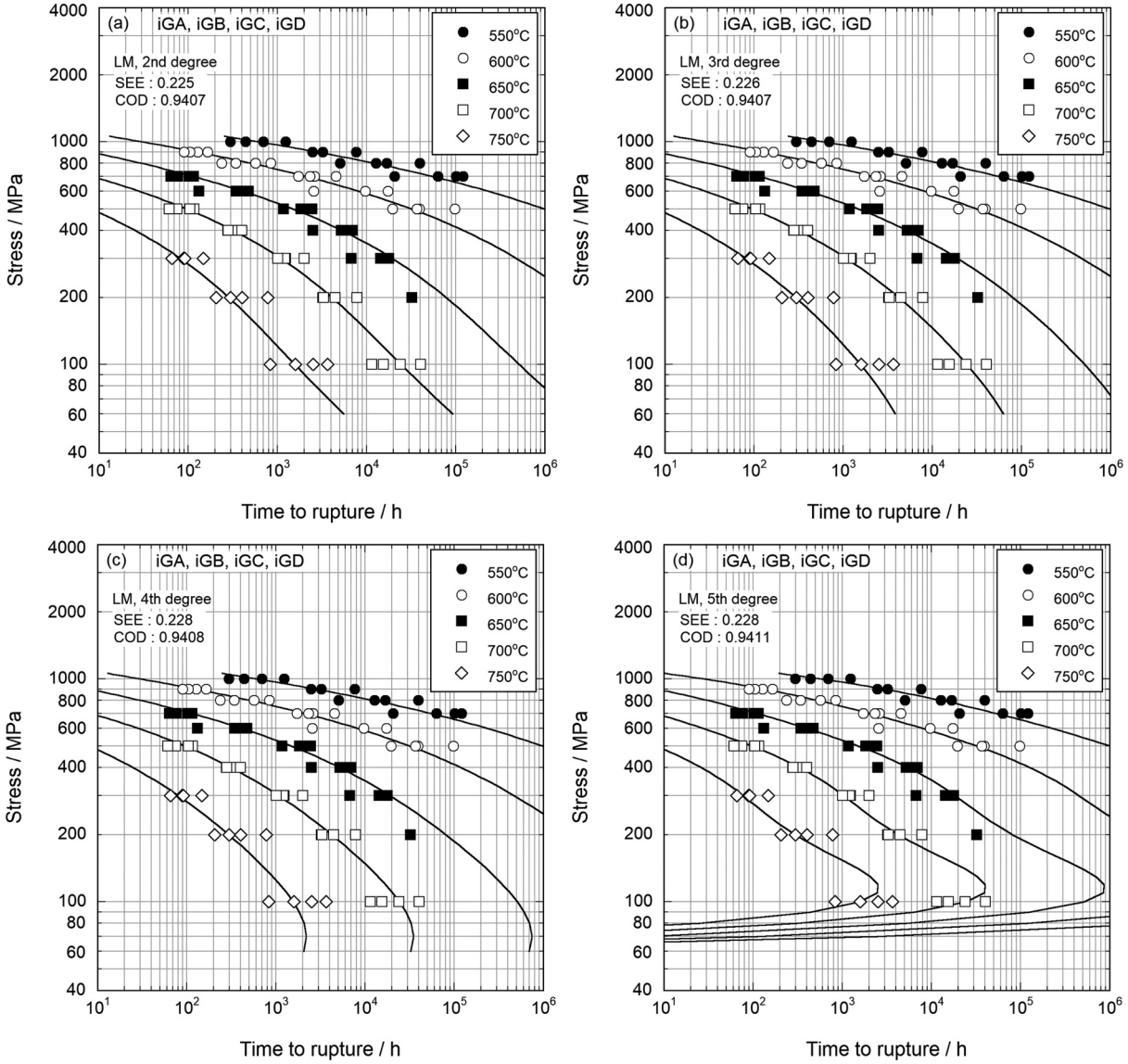

Figure 16. Results of regression analysis by LM parameter and Equation (6). (a)2nd degree, (b) 3rd degree, (c) 4th degree, (d) 5th degree. SEE: standard error of estimate, COD: coefficient of determination.

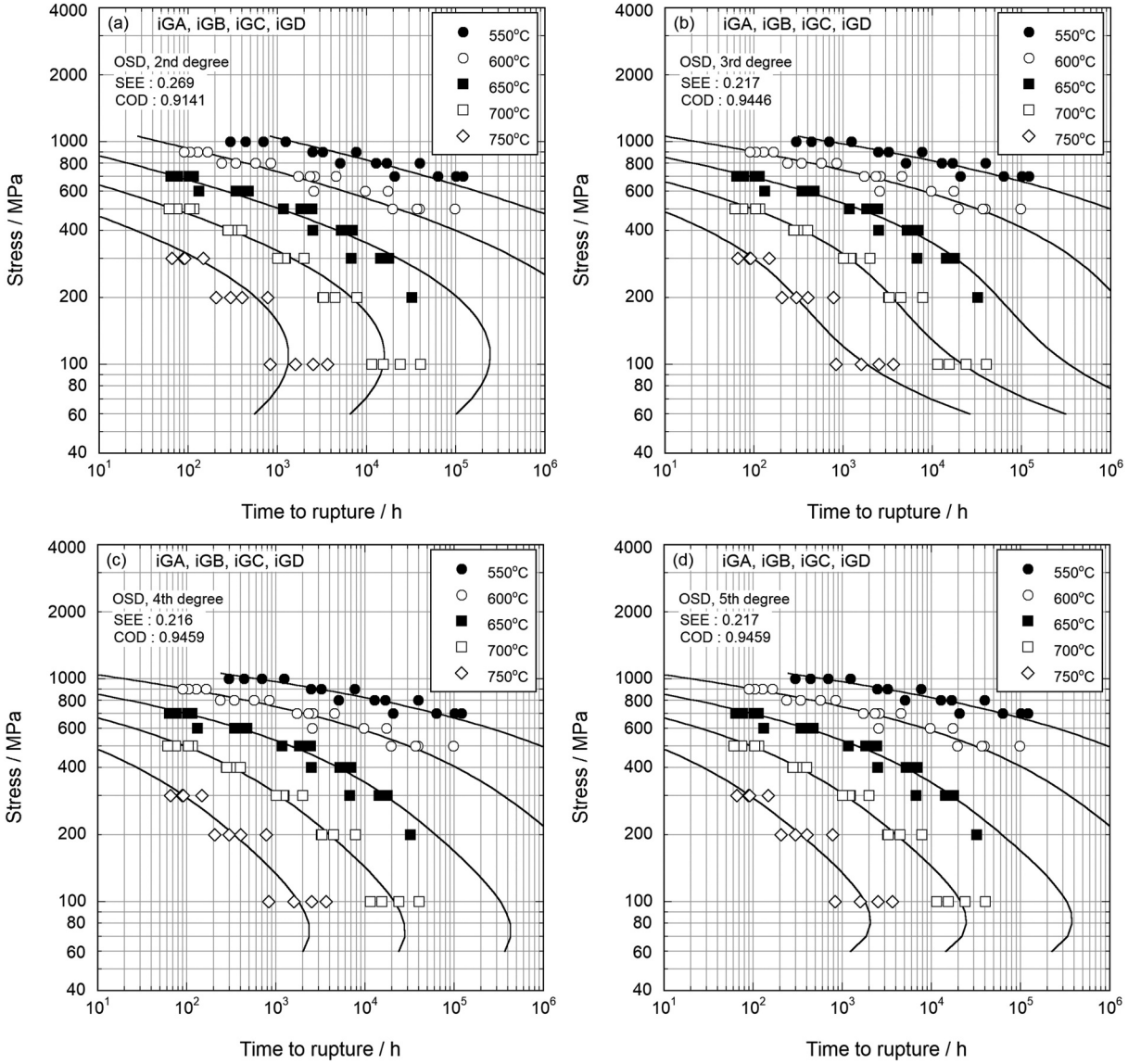

Figure 17. Result of regression analysis by OSD parameter and equation (5). (a) 2nd degree, (b) 3rd degree, (c) 4th degree, (d) 5th degree. SEE: standard error of estimate, COD: coefficient of determination.

term. The fitting curve using the third degree could relatively express the data regardless of the S-shape. In this analysis, the third degree was valid. Figure 18 depicts the results of the regression analysis using the OSD parameter and Eq. (6). The fitting curves using the fourth and fifth degrees were not suitable in the long term. The fitting curves using the second and third degrees seemed to express the data. In this case, the second degree was considered to be suitable because of the simplicity of the equation. Figure 19 shows the results of the regression analysis using the MH parameter and Eq. (5). The fitting curves using the second and fourth degrees could not express the experimental data in the long term. The curves using the third and fifth degrees were relatively suitable for expressing the data compared to the other degrees although the S-shape curve did not agree with the trends of the experimental data in the long term. In this case, the third degree was selected because of the simplicity of the Equation. In the same way as Figure 19, the second degree was selected when the MH parameter and Eq. (6) were used for the analysis (Figure 20). The parameter value of the selected degree for the LM, OSD, and MH parameters are listed in Table 5. For a comparison of the selected curves, the fitting curves using the parameters in Table 5 are shown in Figure 21. At 600°C and 650°C, the fitting curves using the LM parameter overestimated the experimental data in the long term compared with the other parameters. The fitting curves using the MH parameter underestimated the data at 550°C and 600°C in the long term. Therefore, the OSD parameter is suitable for the fitting compared to the LM and MH parameters. The S-shape of the fitting curve using the OSD parameter and Eq. (5) did not match the trends in the experimental data, as shown in Figure 17. Consequently, the fitting curve using the OSD parameter and Eq. (6) was selected for estimating the long-term creep strength of the Ni-based 19Cr-18Fe-3Mo-5Nb-Ti-Al superalloy. Normally, the fitting curves using the OSD and MH parameters tend to underestimate the long-term creep strength compared to

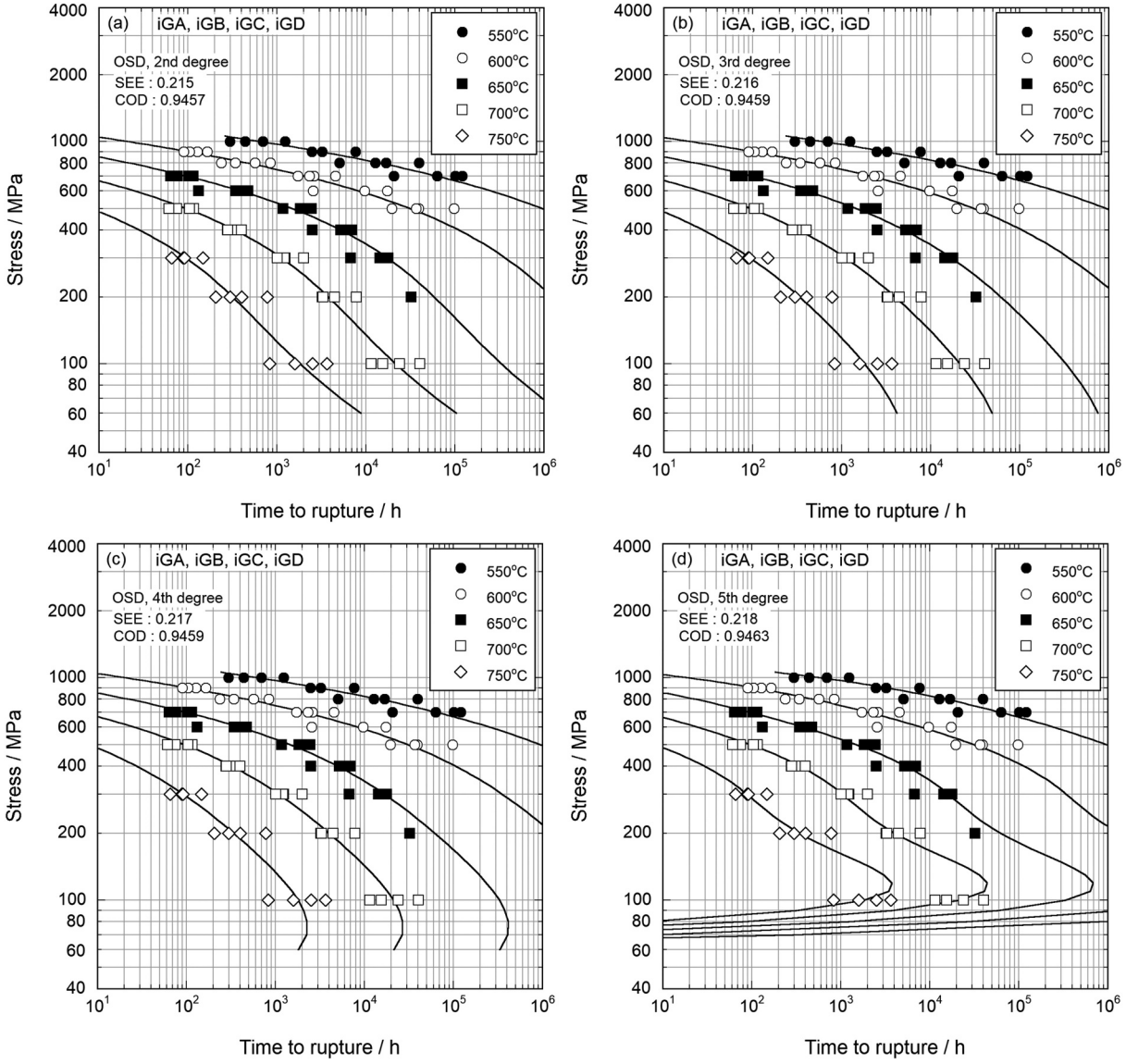

Figure 18. Result of regression analysis by OSD parameter and equation (6). (a) 2nd degree, (b) 3rd degree, (c) 4th degree, (d) 5th degree. SEE: standard error of estimate, COD: coefficient of determination.

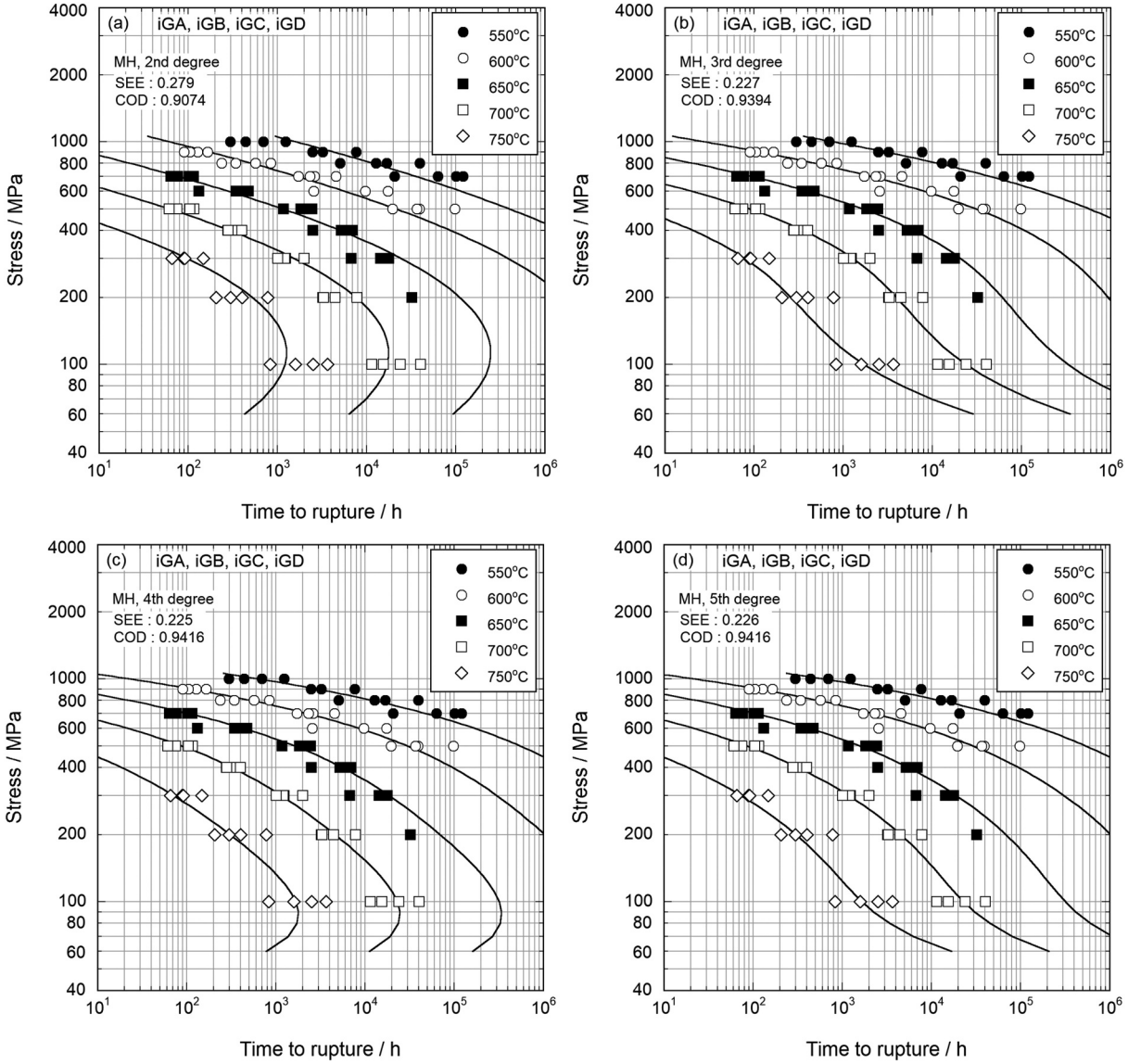

Figure 19. Result of regression analysis by MH parameter and equation (5). (a) 2nd degree, (b) 3rd degree, (c) 4th degree, (d) 5th degree. SEE: standard error of estimate, COD: coefficient of determination.

the LM parameter [17]. In the alloys examined, the γ"-Ni_3Nb and γ'-Ni_3(Al, Ti) particles coarsened during creep exposure, indicating a loss of precipitation strengthening. At 700°C and 750°C, dynamic recrystallization occurred after long-term creep, as shown in Figure 12 This can cause creep strength degradation in the long term. OSD and MH parameters are relatively suitable for creep strength evaluation of materials of which creep strength degrades in the long-term as compared with LM parameter [6]. For Ni-based 21Cr-18Fe-9Mo superalloys, MH parameter was suitable for creep strength evaluation since creep strength degraded in the long-term due to fracture mode change [18]. The regression coefficients of the OSD and Eq. (6) are listed in Table 6. The fitting curves using the regression coefficients are shown in Figure 22. The maximum creep rupture time extrapolated from the data should be less than three times the experimental data. At 550°C and 600°C, the curve was extrapolated up to 300,000 h because the experimental data was obtained up to 100,000 h. In the same way as 550°C and 600°C, the curve was extrapolated up to 100,000 h at 650°C. At 700°C and 750°C, the extrapolation should be up to the time corresponding to 100 MPa because there is no experimental data lower than 100 MPa even at other temperatures. ECCC recommendation [19] says that extended stress extrapolations are those in the ranges $0.9\sigma_{min}$ to σ_{min} and σ_{max} to $1.1\sigma_{max}$. (σ_{min} : minimum stress, σ_{max} : maximum stress) Figure 23 shows the temperature dependence of the 0.2% proof stress, tensile strength, and creep rupture strength at 100, 1,000, 10000, and 100,000 h estimated from the regression equations in Table 6. The value of the creep rupture strength estimated using the regression equations in Table 6 is shown in Table 7. The minimum creep rate data shown in Figure 8 were analyzed and fitted to a regression equation of logarithmic stress using the time – temperature parameter of Orr – Sherby – Dorn

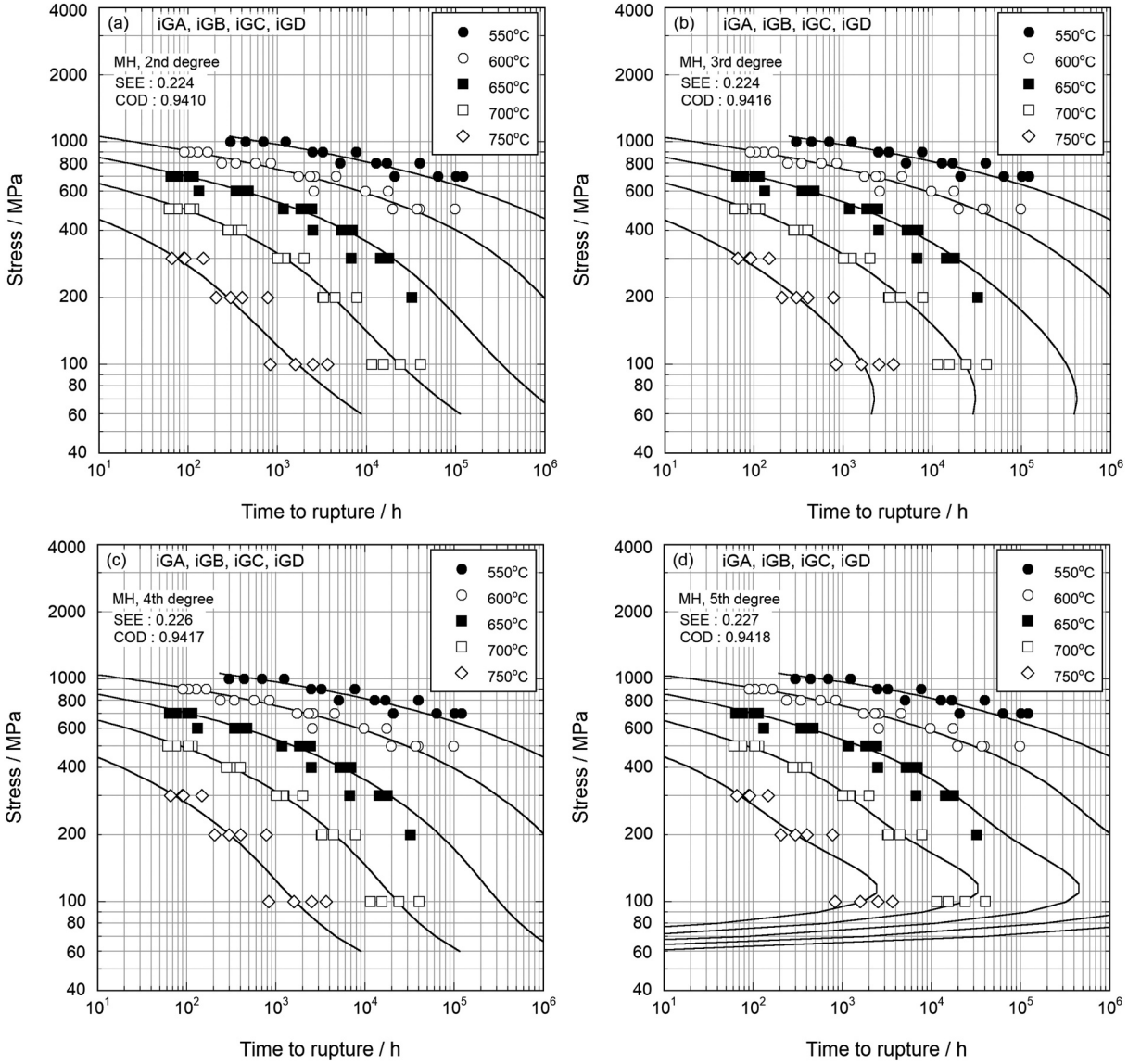

Figure 20. Results of regression analysis by PM parameter and Equation (6). (a)2nd degree, (b) 3rd degree, (c) 4th degree, (d) 5th degree. SEE: standard error of estimate, COD: coefficient of determination.

Table 5. Selected regression coefficient of Laron-Miller, Orr-Sherby-Dorn and Manson-Haferd parameters for creep rupture data.

LM_1 $\log t_R = (T+273.15)^{-1}\,[b + b_1 \log S + b_2(\log S)^2 + b_3(\log S)^3] - C$

LM_2 $\log t_R = (T+273.15)^{-1}\,[b + b_0 S + b_1 \log S + b_2(\log S)^2] - C$

OSD_1 $\log t_R = Q[2.3R(T+273.15)]^{-1} + b + b_1 \log S + b_2(\log S)^2 + b_3(\log S)^3$

OSD_2 $\log t_R = Q[2.3R(T+273.15)]^{-1} + b + b_0 S + b_1 \log S + b_2(\log S)^2$

MH_1 $\log t_R = (T+273.15 - T_a)[b + b_1 \log S + b_2(\log S)^2 + b_3(\log S)^3] + \log t_a$

MH_2 $\log t_R = (T+273.15 - T_a)[b + b_0 S + b_1 \log S + b_2(\log S)^2] + \log t_a$

n*1		C	Q	T_a	$\log t_a$	b_0	b
88	LM_1	2.0082919×10	-	-	-	-	8.1583281×10^4
	LM_2	2.0041082×10	-	-	-	-6.7745789	3.4195860×10^4
	OSD_1	-	4.0967694×10^5	-	-	-	7.0411669×10
	OSD_2	-	4.0880729×10^5	-	-	$-1.0264377 \times 10^{-2}$	2.7875471×10^{-1}
iGA	MH_1	-	-	0.0	2.6674384×10	-	7.3132622×10^{-2}
iGB	MH_2	-	-	0.0	2.6630955×10	$-1.1593576 \times 10^{-5}$	$-3.7221914 \times 10^{-3}$
iGC							
iGD		b_1	b_2	b_3	SEE*2	COD*3	
	LM_1	-7.4381002×10^4	3.2600197×10^4	-4.9249747×10^3	0.226	0.9402	
	LM_2	-8.8697430×10^3	1.9993242×10^3	-	0.225	0.9407	
	OSD_1	-1.1389211×10^2	4.9637668×10	-7.3562705	0.217	0.9446	
	OSD_2	-1.6558838×10	4.0583919	-	0.215	0.9457	
	MH_1	$-1.2493944 \times 10^{-1}$	5.4752822×10^{-2}	$-8.1468562 \times 10^{-3}$	0.227	0.9394	
	MH_2	$-1.7937682 \times 10^{-2}$	4.4716133×10^{-3}	-	0.224	0.9410	

*1 n : number of data points.
*2 SEE : standard error of estimate.
*3 COD : coefficient of determination.
*4 R : gas constant.

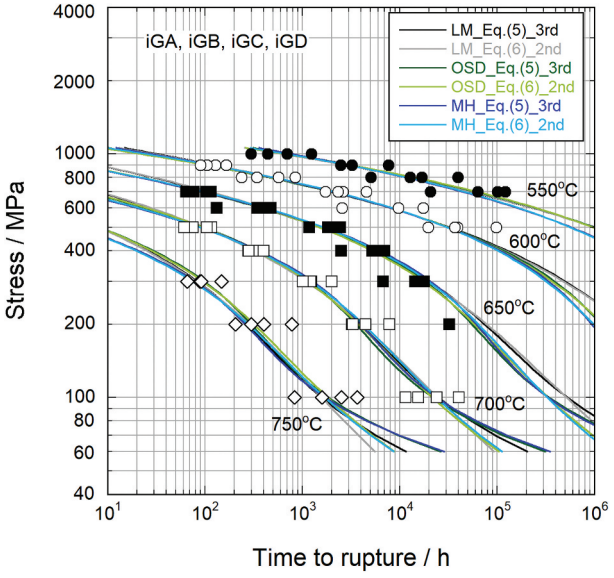

Figure 21. Comparison of fitting curves by LM, OSD and MH parameters.

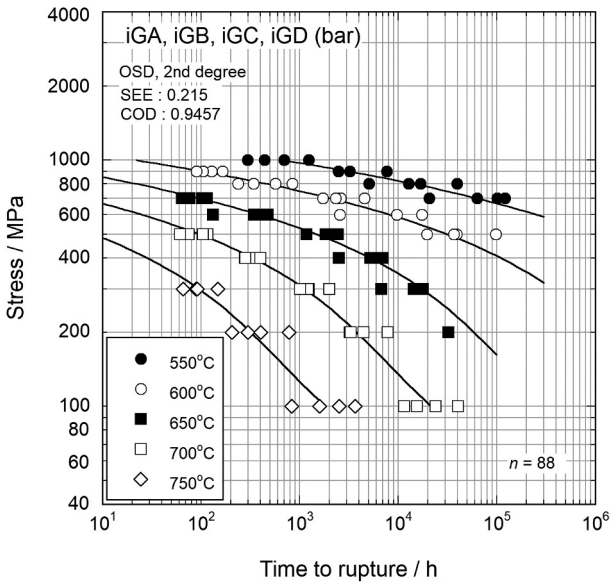

Figure 22. Selected fitting curves by OSD parameter listed in Table 6.

Table 6. Regression coefficient of Orr-Sherby-Dorn parameter for creep rupture data for all heats.

	$\log t_R = Q[2.3R(T+273.15)]^{-1} + b + b_0 S + b_1 \log S + b_2(\log S)^2$				
	n*1	Q	b	b_0	b_1
iGA, iGB iGC, iGD	88	4.0880729×10^5	2.7875471×10^{-1}	$-1.0264377 \times 10^{-2}$	-1.6558838×10
b_2	SEE*2	COD*3			
4.0583919	0.215	0.9457			

*1 n : number of data points.
*2 SEE : standard error of estimate.
*3 COD : coefficient of determination.

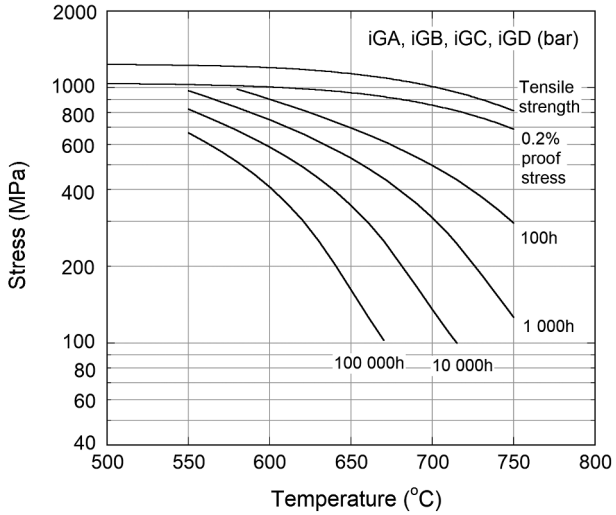

Figure 23. Temperature dependence of 0.2% proof strees, tensile strength and creep rupture strength at 100, 1000, 10000 and 100000h.

Table 7. Summary of creep rupture strength in MPa evaluated from curvilinear regression using Orr-Sherby-Dorn parameter method for Nickel based 19Cr-18Fe-3Mo-5Nb-Ti-Al superalloys.

NIMS reference number	Number of data points	550°C				600°C			
		10^2h	10^3h	10^4h	10^5h	10^2h	10^3h	10^4h	10^5h
iGA, iGB iGC, iGD	88	1119	976	826	668	904	750	587	409
		650°C				700°C			750°C	
		10^2h	10^3h	10^4h	10^5h	10^2h	10^3h	10^4h	10^2h	10^3h
		698	531	347	162	497	310	135	296	126

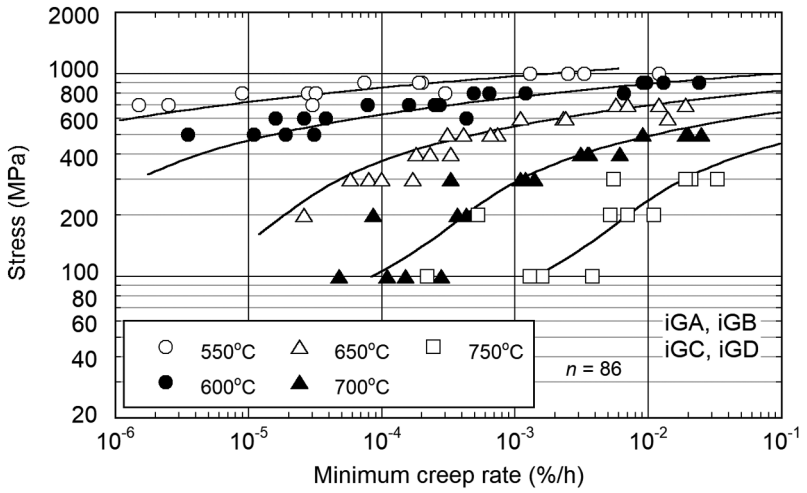

Figure 24. Stress versus minimum creep rate for all heats and fitting curves. The regression equation is given in Table 6.

Table 8. Regression coefficient of Orr-Sherby-Dorn parameter for minimum creep rate data for all heats.

log (minimum creep rate, %/h) = $Q[2.3R(T+273.15)]^{-1} + d + d_0S + d_1 \log S + d_2(\log S)^2$

	n*1	Q	d	d_0
iGA, iGB iGC, iGD	86	-4.6558301×10^5	-1.0414533×10	1.5770086×10^{-2}
	d_1	d_2	SEE*2	COD*3
	3.0352219×10	-7.7331365	0.390	0.8694

*1 n : number of data points.
*2 SEE : standard error of estimate.
*3 COD : coefficient of determination.

in the same way as fitting the creep rupture data. The fitting curve and regression coefficients are shown in Figure 24 and Table 8, respectively.

The data tables used in the present study will be published in a database at https://cds.nims.go.jp/as a NIMS Creep Data Sheet.

6. Conclusions

Short-term tensile and creep rupture data were obtained for four heats of Ni-based 19Cr-18Fe-3Mo-5Nb-Ti-Al superalloy. A regression equation was applied for the analysis of short-term tensile data of the four heats. The creep rupture data at 550°C to 750°C were expressed by a regression equation using the Orr – Sherby – Dorn parameter. It was considered that the heat-to-heat variation in the creep rupture strength was due to the differences in the initial microstructure and microstructural changes during long-term creep exposure.

Disclosure statement

No potential conflict of interest was reported by the author(s).

ORCID

Kota Sawada http://orcid.org/0000-0001-7780-1648
Yasushi Taniuchi http://orcid.org/0000-0002-9988-3370
Kaoru Sekido http://orcid.org/0000-0003-2691-6589
Takehiro Nojima http://orcid.org/0000-0002-1307-2770
Tomotaka Hatakeyama http://orcid.org/0000-0002-2904-8177
Kazuhiro Kimura http://orcid.org/0000-0001-7906-2703

References

[1] American Society of Mechanical Engineers (ASME). ASME boiler and pressure vessel code. Section II. Part D. 2023:1313.
[2] The ministry of economy, trade and industry (METI). The Interpretation For The Technical Standard For Therm Power Plant. 2016:33.
[3] Japanese Standards Association. Japanese industrial standards (JIS). Corrosion-resisting and heat-resisting superalloy bars. JIS G 4901. 1999:2.
[4] Japanese Standards Association. Japanese industrial standards (JIS). Method of elevated temperature tensile test for steels and heat-resisting alloys. JIS G 0567;1998:1–13.
[5] Japanese Standards Association. Japanese industrial standards (JIS). Method of creep and creep rupture test for metallic materials. JIS Z 2271. 1998:1–17.
[6] Sawada K, Taniuchi Y, Sekido K, et al. Creep properties and analysis of creep rupture data of 2.25Cr-1Mo-0.3V steels. Sci Tech Adv Mater Methods. 2022;2 (1):198–212. doi: 10.1080/27660400.2022.2080484
[7] Preston-Thomas H. The international temperature scale of 1990 (ITS-90). Metrologia. Metrologia. 1990;27(1):3–10. doi: 10.1088/0026-1394/27/1/002
[8] R LF, Miller J. A time-temperature relationship for rupture and creep stresses. Trans ASME. 1952;74 (5):765–771. doi: 10.1115/1.4015909
[9] Orr RL, Sherby OD, Dorn JE. Correlations of rupture data for metals at elevated temperatures. Trans ASM. 1954;46:113–118.
[10] Manson SS, Haferd A. A linear time-temperature relation for extrapolation of creep and stress rupture data. Washington: National Advisory Committee for Aeronautics; 1953. p. TN2890.
[11] Haque MS, Stewart CM. Metamodeling time-temperature creep parameters. J Press Vessel Technol. 2020;142(3):031504. doi: 10.1115/1.4045887
[12] Sawada K, Sekido K, Kimura K, et al. Effect of initial microstructure on creep strength of ASME grade T91 steel. ISIJ Int. 2020;60(2):382–391. doi: 10.2355/isijinternational.ISIJINT-2019-358
[13] Johnson WR, Barrett CR, Nix WD. The effect of environment and grain size on the creep behavior of a Ni-6Pct W solid solution. Metall Trans. 1972;3 (3):695–698. doi: 10.1007/BF02642753
[14] Maruyama K, Nakamura J, Sekido N, et al. Causes of heat-to-heat variation of creep strength in grade 91 steel. Mater Sci Eng A. 2017;696:104–112. doi: 10.1016/j.msea.2017.04.050
[15] Monkman FC, Grant. The procedure fair. N J Proc ASTM. 1956;56(5):593–597. doi: 10.2307/3469318
[16] Brooks JW, Bridges PJ. Metallurgical stability of Inconel alloy 718. In: Reichman S, N DD, Maurer G, Antolovich S Lund C, editors. Proceedings of 6th International Conference Superalloys; Champion (PA). The Metallurgical Society; 1988. p. 33–42. [1988 Sept 18–22].
[17] Maruyama K, Baba E, Yokokawa K, et al. Errors of creep rupture life extrapolated by time-temperature parameter methods. Tetsu-To-Hagane. 1994;80 (4):336–341. doi: 10.2355/tetsutohagane1955.80.4_336
[18] Sawada K, Taniuchi Y, Sekido K, et al. Long-term creep properties of Ni-based 21Cr-18Fe-9Mo superalloys. Sci Tech Adv Mater Methods. 2023;3(1):2284129. doi: 10.1080/27660400.2023.2284129
[19] Farrugia A, Vamvakas E., ECCC Recommendations. Toward a patient-based paradigm for blood transfusion. J Blood Med. 2014;Volume 5 Part Ia Issue 6;5–13. doi: 10.2147/JBM.S55769